

Dipole-dipole instability of atom clouds in a far-detuned optical dipole trap

D. Nagy and P. Domokos

*Research Institute of Solid State Physics and Optics,
Hungarian Academy of Sciences, H-1525 Budapest P.O. Box 49, Hungary*

The effect of the dipole-dipole interaction on the far-off-resonance optical dipole trapping scheme is calculated by a mean-field approach. The trapping laser field polarizes the atoms and the accompanying dipole-dipole energy shift deepens the attractive potential minimum in a pancake-shaped cloud. At high density the thermal motion cannot stabilize the gas against self-contraction and an instability occurs. We calculate the boundary of the stable and unstable equilibrium regions on a two-dimensional phase diagram of the atom number and the ratio of the trap depth to the temperature.

I. INTRODUCTION

The optical dipole trap provides a conservative and tightly confining trapping potential for polarizable particles. Owing to its simplicity it has become a standard tool for manipulating neutral atoms [1]. Today, various dipole trap based systems serve the study of many-body problems where the atom-atom interaction is an essential ingredient. In this paper we consider far-off-resonant trapping of polarizable particles interacting radiatively through the electromagnetic vacuum field.

In dense samples of cold atoms, two-atom processes strongly influence the trapping. For example, collisional processes (photo-association, hyperfine ground state changing collisions, etc.) are known to result in trap losses and they can limit the maximum achievable density. Collisions usually depend heavily on the internal electronic structure of the species. For interatomic distances in the range of the optical wavelength, the atom-atom interaction is dominated by the radiative electromagnetic coupling. In this case one can distinguish two limits: the photon scattering is dominated (i) by spontaneous emission, e.g. in magneto-optical traps (MOT), and (ii) by stimulated emission, which occurs in far-off-resonant dipole traps (FORT). Since the MOT was the first to be able to capture dense atom clouds from vapour, it was first analyzed with respect to many-body effects [2, 3]. In a MOT, the cooling laser is quasi-resonant with the atoms and the sample forms an optically thick medium. The depletion of the laser beams together with the multiple spontaneous scattering of resonant photons within the sample can lead to instability [2] and extra heating [4, 5]. At high densities, the reabsorption of photons influences the laser cooling itself [6, 7]. The combination of these effects can result in a highly nonlinear collective dynamics of the atom cloud in a MOT [8, 9].

The FORT operates at an extremely low spontaneous scattering rate, thus the effects of multiple spontaneous photon scattering are strongly suppressed. The mechanism of trapping relies on the process of absorption and stimulated emission of laser photons. This process polarizes the particles, hence the dipole force is accompanied by the conservative dipole-dipole coupling between atoms.

It is a formidable task to include all the atom-atom couplings at a microscopic level. In previous works a phenomenological term proportional to the square of the atom density was introduced to describe the atom-atom interaction, e.g., the effect of collisions on the loading of a FORT [10, 11]. This dominates in strongly localized traps, collisional blockade can prevent us from confining even two atoms in an extremely tiny FORT [12]. This paper is devoted to studying, based on a microscopic theory, the radiative interaction between atoms in a FORT. We explore constraints limiting the maximum achievable density in a FORT, which arise solely from the dipole-dipole energy shift. We will refrain from a detailed modeling of the collisions and will exclude, by assuming a hard sphere potential, the domain of distances where the Coulomb and exchange interaction terms require the use of molecular potential surfaces [13].

Tuning the laser frequency ω_L very far below the atomic resonance ω_A makes it possible to eliminate the spontaneous photon scattering at a constant depth of the trap potential, since the scattering rate and the trap depth scale differently with the detuning $\Delta_A = \omega_L - \omega_A$. The former is proportional to $2\gamma\Omega^2/\Delta_A^2$ while the latter to Ω^2/Δ_A where Ω is the Rabi frequency of the atom-laser coupling, γ is the atomic linewidth (HWHM). Assuming temperatures well below the potential depth, i.e., $(\hbar\Omega^2/\Delta_A)/(k_B T) \gg 1$, the particles are captured in the trap for long times. The dipole-dipole energy shift scales similarly to the spontaneous scattering rate, however, it is enhanced by the atom density. Thus it may become significant as compared to the dipole trap depth when the atom number N obeys $N\gamma/\Delta_A \gtrsim 0.1$ in the trapped cloud.

High atom densities can be an issue for many kinds of experiments with FORT's, therefore our goal is to treat this problem in as general a way as possible. One example is the attempt to achieve Bose-Einstein condensation with alkali gases in optical rather than magnetic traps [14, 15]. Another example is connected to the so-called *cavity cooling* method which is suitable to complement the deep conservative potential of FORT by a damping force induced by the field of a high-finesse optical resonator [16, 17]. Various cavity cooling setups have been realized: (i) the FORT field can be along the cavity axis

and detuned from the near-resonant cavity field by several free spectral ranges [18, 19]; or the FORT lasers can be perpendicular to the cavity axis with photons scattered into the cavity responsible for cooling [20, 21]. The simultaneous cooling and trapping gives rise to very long trapping times for single atoms. Cavity cooling can be applied to many atoms as well, and should work efficiently until they get localized at the antinodes of the red detuned trap field [22, 23, 24].

The paper is organized as follows. We start by recapitulating the formulae of the dipole-dipole interaction of atoms at a microscopic level in Sec. II. Then, in Sec. III we take the far-off-resonance limit and keep only the leading order terms in the small parameter γ/Δ_A . During this limiting procedure we have to treat the density-enhanced terms by a systematic expansion and keep only the two-body terms. The basic equations of the mean-field model are introduced in Sec. IV. These can be expressed in terms of dimensionless parameters, the scaled intensity and the scaled atom number, which define the universality of this model. Section V is devoted to the discussion of the trap geometry. For computational convenience, we perform the numerical calculations for smaller spatial sizes than that of realistic traps. We present the results of the stability analysis in Sec. VI. There we show the parameter regimes (laser intensity and atom number) of stability and instability on phase diagrams and discuss the sensitivity of these phase diagrams with respect to the model parameters. We conclude in Sec. VII.

II. DIPOLE-DIPOLE INTERACTION

We consider a number N of atoms interacting with a single Gaussian standing-wave laser field mode which has a mode function near the center of the beam

$$\vec{f}(\vec{r}) = \vec{\epsilon} \cos(k_z z) \exp[-2\pi^2(x^2 + y^2)/w^2]. \quad (1)$$

Here light propagates in the \hat{z} direction, $\vec{\epsilon}$ is the field polarization, and the mode is paraxial, $k_z \gg 2\pi/w$. The atomic transition frequency is ω_A , that of the laser field mode is ω_L , and the detuning is defined by $\Delta_A = \omega_L - \omega_A$. The atom-mode interaction strength is described by the Rabi frequency Ω in the position of maximum coupling. We assume an $S \leftrightarrow P$ transition with a degenerate manifold of excited states and keep the three-dimensional polarizability of the atoms. Actually the fixed field polarization selects two levels taking part in the dynamics. The atomic internal degree of freedom is described by the vectorial lowering operator $\vec{\sigma} = \sum_q \vec{\epsilon}_q \sigma^q$ with $q = \pm 1$ and $q = 0$ corresponding to the circular and linear polarizations, respectively. The quantization axis will be defined in accordance with the choice of the field polarization $\vec{\epsilon}$.

The equation of motion for the density operator in the Markoff approximation reads

$$\rho = \frac{1}{i\hbar} [H, \rho] + \mathcal{L}\rho. \quad (2)$$

In a frame rotating at the laser frequency ω_L , the Hamiltonian is

$$H = \sum_{n=1}^N \left[\frac{\vec{p}_n^2}{2m} - \hbar \Delta_A \vec{\sigma}_n^\dagger \vec{\sigma}_n - i\hbar\Omega \vec{f}(\vec{r}_n) (\vec{\sigma}_n^\dagger - \vec{\sigma}_n) \right] - \hbar\gamma \sum_{\substack{n,m=1 \\ n \neq m}}^N \vec{\sigma}_m^\dagger \beta(\vec{R}_{mn}) \vec{\sigma}_n, \quad (3)$$

where \vec{r}_n , \vec{p}_n and $\vec{\sigma}_n$ are the position, the momentum and the polarization of the n th atom ($n = 1, \dots, N$). Next to the single atom terms, i.e. kinetic energy, internal energy, and atom-field coupling, the last term contains the induced dipole-dipole interaction energy of the atoms. Note that the natural linewidth γ characterizes the strength of this interaction. The tensor β depends on the coordinate difference $\vec{R}_{mn} \equiv \vec{r}_m - \vec{r}_n$ of the interacting pairs of atoms.

The dipole-dipole interaction is mediated by the broadband vacuum, and is therefore accompanied by incoherent evolution. This is represented by additional terms in the Liouville operator responsible for the dissipation [25]:

$$\begin{aligned} \mathcal{L}\rho = & -\gamma \sum_{n=1}^N (\{\vec{\sigma}_n^\dagger \vec{\sigma}_n, \rho\} - \\ & - 2 \sum_q \int d^2 \vec{u} N_q(\vec{u}) \sigma_n^q e^{-ik_A \vec{u} \cdot \vec{r}_n} \rho e^{ik_A \vec{u} \cdot \vec{r}_n} \sigma_n^{q\dagger}) \\ & - \gamma \sum_{\substack{n,m=1 \\ n \neq m}}^N (\{\vec{\sigma}_m^\dagger \alpha(\vec{R}_{mn}) \vec{\sigma}_n, \rho\} - \\ & - 2 \int d^2 \vec{u} \vec{\sigma}_n \mathbf{N}(\vec{u}) e^{-ik_A \vec{u} \cdot \vec{r}_n} \rho e^{ik_A \vec{u} \cdot \vec{r}_m} \vec{\sigma}_m^\dagger), \quad (4) \end{aligned}$$

where $\{\cdot, \cdot\}$ denotes the anticommutator. The single atom terms include the spontaneous decay accompanied by momentum recoil. The tensor $\mathbf{N}(\vec{u}) = \frac{3\gamma}{8\pi} (1 - \vec{u} \circ \vec{u})$, and its diagonal elements $N_q(\vec{u}) = \vec{\epsilon}_q^\dagger \mathbf{N}(\vec{u}) \vec{\epsilon}_q$ are the angular momentum distribution of the spontaneous emission from the q -state in the excited manifold. The double sum describes the loss effect due to the dipole-dipole coupling.

In free space the tensors α and β assume the following form [7, 25, 26] :

$$\begin{aligned} \alpha(\vec{R}_{mn}) = & \frac{3}{2} \left\{ (1 - \hat{R}_{mn} \circ \hat{R}_{mn}) \frac{\sin kR_{mn}}{kR_{mn}} \right. \\ & \left. + (1 - 3\hat{R}_{mn} \circ \hat{R}_{mn}) \left(\frac{\cos kR_{mn}}{(kR_{mn})^2} - \frac{\sin kR_{mn}}{(kR_{mn})^3} \right) \right\}, \quad (5) \end{aligned}$$

$$\begin{aligned} \beta(\vec{R}_{mn}) = & \frac{3}{2} \left\{ (1 - \hat{R}_{mn} \circ \hat{R}_{mn}) \frac{\cos kR_{mn}}{kR_{mn}} \right. \\ & \left. - (1 - 3\hat{R}_{mn} \circ \hat{R}_{mn}) \left(\frac{\sin kR_{mn}}{(kR_{mn})^2} + \frac{\cos kR_{mn}}{(kR_{mn})^3} \right) \right\}, \quad (6) \end{aligned}$$

where $k = |\vec{k}| \approx k_z$, $R_{mn} = |\vec{R}_{mn}|$, and \hat{R}_{mn} is a unit vector along the direction of \vec{R}_{mn} .

The fixed field polarization selects the excited state and the atom reduces to a two-level system with $\vec{\sigma}_n = \sigma_n \vec{\epsilon}$ ($n = 1, \dots, N$). The tensors $\boldsymbol{\alpha}$ and $\boldsymbol{\beta}$ have to be projected onto this particular polarization,

$$\vec{\sigma}_m^\dagger \boldsymbol{\beta}(\vec{R}_{mn}) \vec{\sigma}_n = \beta(\vec{R}_{mn}) \sigma_m^\dagger \sigma_n, \quad (7)$$

where $\beta(\vec{R}_{mn}) = \vec{\epsilon}^\dagger \boldsymbol{\beta}(\vec{R}_{mn}) \vec{\epsilon}$. We now evaluate this projection in two cases: for linear polarization along \hat{x} , and for circular one in the \hat{x} – \hat{y} plane.

A. Linear polarization

When the polarization of the beam is linear, $\vec{\epsilon} = \hat{x}$, the atomic quantization axis is taken in this direction. The atomic polarization is described by the operator σ_0 , and the projection given in Eq. (7) results in

$$\begin{aligned} \beta_{mn} = \frac{1}{2} (3 \cos^2 \phi_{mn} - 1) & \left[\frac{\sin kR_{mn}}{(kR_{mn})^2} + \frac{\cos kR_{mn}}{(kR_{mn})^3} \right] \\ & + \frac{3}{2} (1 - \cos^2 \phi_{mn}) \frac{\cos kR_{mn}}{kR_{mn}}, \end{aligned} \quad (8)$$

where $\phi_{mn} = \angle(\vec{R}_{mn}, \hat{x})$ is the angle between the distance vector of the two atoms and the axis of the polarization, \hat{x} .

B. Circular polarization

If the polarization is circular, $\vec{\epsilon} = -\frac{1}{\sqrt{2}}(\hat{x} + i\hat{y})$, the atomic quantization axis is the field propagation direction \hat{z} . The atomic polarization is described by the operator σ^{+1} , and the projection Eq. (7) gives

$$\begin{aligned} \beta_{mn} = \frac{3}{4} (1 - 3 \cos^2 \theta_{mn}) & \left[\frac{\sin kR_{mn}}{(kR_{mn})^2} + \frac{\cos kR_{mn}}{(kR_{mn})^3} \right] \\ & + \frac{3}{4} (\cos^2 \theta_{mn} + 1) \frac{\cos kR_{mn}}{kR_{mn}}. \end{aligned} \quad (9)$$

The angle $\theta_{mn} = \angle(\vec{R}_{mn}, \hat{z})$ is the angle between the distance vector of the two atoms and the axis \hat{z} .

III. LARGE DETUNING LIMIT

For red detuning ($\Delta_A < 0$) the atoms are attracted to high-intensity regions of the field. In the large detuning limit, i.e., where the magnitude of Δ_A exceeds the atomic linewidth γ by far, $|\Delta_A| \gg \gamma$, the laser field creates a conservative potential for the atoms. The recoil noise is so strongly suppressed that heating plays no role on the relevant timescale of motion. It is enough to consider only

the conservative part of the dynamics described by the Hamiltonian. The dissipative processes will be taken into account later by the introduction of a phenomenological temperature.

The internal electronic dynamics of the atoms consists of fast oscillations on a short timescale. This can be adiabatically eliminated to derive its effect on the external motion. The adiabatic atomic polarizations, according to Eq. (3), obey the implicit equation

$$\sigma_n = \frac{\Omega}{\Delta_A} f(\vec{r}_n) + \frac{\gamma}{\Delta_A} \sum_{\substack{m=1 \\ m \neq n}}^N \Theta_{mn} \sigma_m, \quad (10)$$

where $\Theta_{mn} = \alpha_{mn} - i\beta_{mn}$ has been introduced for the sake of compactness of this and the next equation. Eq. (10) can be solved iteratively to obtain

$$\begin{aligned} \frac{\Delta_A \sigma_n}{\Omega} = f(\vec{r}_n) & + \frac{\gamma}{\Delta_A} \sum_{\substack{m=1 \\ m \neq n}}^N \Theta_{nm} f(\vec{r}_m) \\ & + \left(\frac{\gamma}{\Delta_A} \right)^2 \sum_{\substack{m=1 \\ m \neq n}}^N \sum_{\substack{l=1 \\ l \neq m}}^N \Theta_{nm} \Theta_{ml} f(\vec{r}_l) \\ & + \left(\frac{\gamma}{\Delta_A} \right)^3 \sum_{\substack{m=1 \\ m \neq n}}^N \sum_{\substack{l=1 \\ l \neq m}}^N \sum_{\substack{k=1 \\ k \neq l}}^N \Theta_{nm} \Theta_{ml} \Theta_{lk} f(\vec{r}_k) + \dots \end{aligned} \quad (11)$$

The series includes terms of high order in the small parameter $\gamma/|\Delta_A| \ll 1$, however, not all of them can be neglected. Such a high-order term can contain extremely large factors provided all the Θ_{kl} in it have large values, i.e., the corresponding atoms all are close to each other (within a small fraction of the wavelength). This is because in the limit $R_{mn} \rightarrow 0$, the dipole-dipole coupling function gives $\beta(\vec{R}_{mn}) \rightarrow \infty$. However, even in this limit α is bounded, i.e. $\alpha(\vec{R}_{mn}) \rightarrow 1$, thus the real part of Θ can safely be neglected in the large detuning limit.

A systematic low-density approximation of Eq. (11) can be made by considering only two-body terms. This amounts to the assumption that any pair of atoms can be very closely spaced, however, in this case there is no third atom in their immediate vicinity. Thus if for any $n \neq m$, $\beta_{nm} \gg 1$, then for every $l = 1, \dots, N$ such that $l \neq n$, $l \neq m$, we have $\beta_{nm} \beta_{ml} \leq 1$. In this approximation, we reorder the sum, and obtain two geometric series of $-\beta_{mn} \gamma / \Delta_A$, leading to

$$\begin{aligned} \sigma_n = \frac{\Omega}{\Delta_A} \left[\left(1 + \sum_{\substack{m=1 \\ m \neq n}} \frac{(\beta_{mn} \gamma / \Delta_A)^2}{1 - (\beta_{mn} \gamma / \Delta_A)^2} \right) f(\vec{r}_n) \right. \\ \left. - \sum_{\substack{m=1 \\ m \neq n}} \frac{(\beta_{mn} \gamma / \Delta_A)}{1 - (\beta_{mn} \gamma / \Delta_A)^2} f(\vec{r}_m) \right]. \end{aligned} \quad (12)$$

Here we have assumed that for every atom pair $n \neq m$, $|\beta_{mn} \gamma / \Delta_A| < 1$. This solution, within the Markoff and

the adiabatic approximations, takes into account in a non-perturbative manner the pairs of atoms separated by small distances.

Inserting the stationary atomic polarization Eq. (12) back into the Hamiltonian Eq. (3), and eliminating double sums on the same ground as above yields an effective two-body Hamiltonian H_{eff} given in the Appendix. To leading order in $|\beta_{mn}\gamma/\Delta_A|$, the polarization is $\sigma_n = f(\vec{r}_n)\Omega/\Delta_A$, which gives the zeroth order of the full effective Hamiltonian:

$$H_{\text{eff}}^{(0)} = \sum_{n=1}^N \left(\frac{\vec{p}_n^2}{2m} + \frac{\hbar\Omega^2}{\Delta_A} f^2(\vec{r}_n) \right) - \frac{\hbar\gamma\Omega^2}{\Delta_A^2} \sum_{\substack{n,m \\ n \neq m}}^N \beta(\vec{r}_n - \vec{r}_m) f(\vec{r}_n) f(\vec{r}_m). \quad (13)$$

This Hamiltonian $H_{\text{eff}}^{(0)}$ describes the dynamics of dipolar particles, where the polarization is induced by the external driving field. The neglected higher order terms describe the effect of one polarized particle on the polarization of another, i.e., the *local field effects*. The same effect is at the heart of the Lorenz-Lorentz refractive index of a dielectric medium. We will later discuss in which parameter regime the local field effects become significant.

IV. MEAN-FIELD APPROXIMATION

In the following we will resort to an effective single-atom analysis based on a mean-field potential. In order to simplify the expressions, in this section we will use the Hamiltonian in Eq. (13), which is a first order expression in $\beta_{mn}\gamma/\Delta_A$. The conservative dipole trap potential is

$$V_{\text{trap}}(\vec{r}) = \frac{\hbar\Omega^2}{\Delta_A} f^2(\vec{r}). \quad (14)$$

The mean-field dipole-dipole potential is

$$V_{\text{dd}}^{(0)}(\vec{r}) = -2\hbar\gamma \frac{\Omega^2}{\Delta_A^2} f(\vec{r}) \int d^3\vec{r}_2 p(\vec{r}_2) \beta(\vec{r} - \vec{r}_2) f(\vec{r}_2), \quad (15)$$

where the continuous position distribution $p(\vec{r})$ was introduced. This distribution is normalized to the number of atoms in the trap N . A similar conservative dipole-dipole MF potential has been studied in the case of the Gross-Pitaevski equation for degenerate ultracold atoms [27, 28].

In the limit of $R_{mn} \rightarrow 0$, one can distinguish two orders of magnitude in the expression of β_{mn} in Eq. (8) and Eq. (9). The largest order is proportional to $(kR_{mn})^{-3}$, that is followed by the terms scaling with $(kR_{mn})^{-1}$. Because of the former, the dipole-dipole interaction energy is divergent, thus we have to exclude a region around the position \vec{r} of the atom. We introduce a hard sphere

potential with radius r_0 , mimicking the real collisional mechanism between the atoms. For a given detuning Δ_A , the radius r_0 must be chosen such that $|\beta(r_0)\gamma/\Delta_A| < 1$, so that the iterative solution in Eq. (11) is convergent. On the other hand, to be consistent with omitting the collisions, r_0 must be larger than the scattering length of the atoms. It can then be chosen in the order of the hundredth of a wavelength, i.e., $kr_0 \ll 1$.

The final step in setting up the model consists of assuming that the cloud of atoms is described by a canonical ensemble at an equilibrium temperature T . By this approximation we avoid describing the heating and cooling processes which lead to the steady-state. Both are slow processes as the recoil noise is strongly suppressed. The canonical distribution provides a self-consistent equation for the spatial distribution of the atoms:

$$p(\vec{r}) = \frac{1}{\mathcal{Z}} \exp \left[-\frac{V(\vec{r}, p(\vec{r}))}{k_B T} \right], \quad (16)$$

where the partition function \mathcal{Z} ensures that the integral of $p(x)$ gives the number N of atoms. This self-consistent equation for the atom distribution is the basic equation of our model, which can be solved only numerically. The same method has been used to study phase transitions of atom gases when the atom-atom interaction is mediated by a cavity field [24, 29].

The MF model can be expressed in terms of dimensionless parameters, which amounts to the identification of the relevant quantities describing the equilibrium of a trapped cloud of atoms. The dipole trap depth (see Eq. (14)) is set by the intensity and the detuning, however, in the self-consistent equation (16) it is compared to the temperature. None of the above quantities appears separately, thus it is appropriate to introduce the scaled intensity

$$\mathcal{I} = \frac{\hbar\Omega^2}{|\Delta_A| k_B T}. \quad (17)$$

The depth of the MF dipole-dipole potential relative to the trap depth is determined by the product of the small parameter γ/Δ_A and the atom number N through the atomic density $p(\vec{r})$ in Eq. (15). The appropriate parameter is then the scaled atom number

$$\mathcal{N} = \frac{N\gamma}{|\Delta_A|}. \quad (18)$$

With these two dimensionless parameters, \mathcal{I} and \mathcal{N} , the effect of all the relevant physical quantities can be described.

V. TRAP GEOMETRY

The difficulty of solving numerically Eq. (16) stems from the necessity of bridging over two different length scales. One is the spatial resolution imposed by the cutoff

parameter r_0 . This is strongly dependent on the atomic species and we employ phenomenological values in the range of 10-100 nm. The other is the geometrical size of the trap, given by the Gaussian beam waist w in the transverse direction and the wavelength λ in the axial one. Typically $w \gg \lambda$, thus the mode function Eq. (1) creates a pancake-shaped cloud compressed along the \hat{z} axis.

The mean field dipole-dipole energy Eq. (15) depends on the shape of the atomic cloud. It vanishes in the center for a spherical atom distribution (the refinement of this statement in the case when there is no excluded volume around the origin can be found in [30]). In the fictitious limiting case of $\mathcal{I} = \infty$ the atoms are trapped in the harmonic domain both along the cosine mode function and transversely along the Gaussian beam envelope. In this limit the cloud is spherical $w = \lambda$. For finite intensity there is anharmonicity, different in the orthogonal directions, and the MF dipole-dipole energy vanishes at slightly smaller w .

In an anisotropic pancake-shaped cloud, the dipole-dipole contribution to the MF potential is negative, deepening the trap depth in the center. We numerically tested that choosing a waist as small as $w \geq 1.33\lambda$ can account for the general property of having dipole-dipole attraction in the trap center. Therefore it is possible to consider an unrealistically small waist, $w/\lambda \sim 1.33$, which leads to saving significant computation time without essentially modifying the results.

We note that for a cigar-shaped cloud the MF dipole-dipole energy would be positive, repelling atoms from the center, and thus the instability we discuss in the following could not occur.

VI. STABILITY ANALYSIS

The solution of Eq. (16) can be determined numerically by iterating the atomic distribution as follows. Starting from a homogeneous cloud, we calculate the dipole-dipole interaction term. This requires the evaluation of an integral similar to Eq. (15), but using the non-perturbative two-body potential term of the Hamiltonian in Eq. (19). This dipole-dipole term added to the dipole trap term of Eq. (14) yields the total mean field potential which furnishes a new atomic distribution via the canonical form in Eq. (16). The resulting $p(x)$ can be used as the starting distribution in the next step of the iteration. Continuing the steps of iteration until convergence, one obtains the self-consistent solution of Eq. (16). The iteration does not necessarily converge: instability can be induced by large enough atom number or intensity. The iteration method suggests that the instability occurs as a collapse of the atomic cloud due to self-contraction in the center of the trap. However, in the lack of a precise modeling of the collisional processes, the collapse itself cannot be accounted for by our approach. We must limit ourselves to determining the range of convergence.

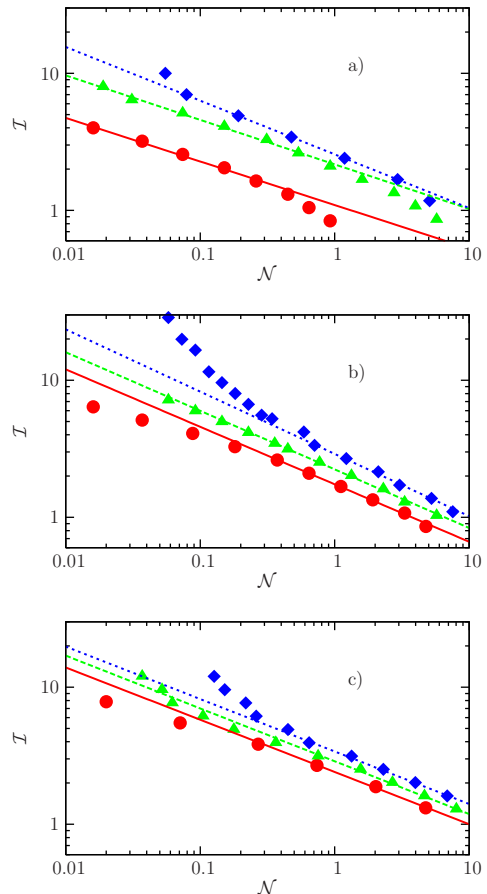


FIG. 1: The stability limit of the atomic cloud is shown in logarithmic phase diagram of the scaled intensity \mathcal{I} and the scaled atom number \mathcal{N} . The field polarization is (a) linear along the axis \hat{x} , (b) circular in the $\hat{x} - \hat{y}$ plane, and for both plots the waist is $w = 1.33\lambda$. We compare atoms with different cutoff parameters, $r_0/\lambda = 0.02$ (circles), 0.04 (triangles), and 0.08 (diamonds). The parameters for figure (c) are the same as for (b) only the beam waist is larger, $w = 2.22\lambda$.

In Fig. 1 the stability range of the iterations is presented for the case of (a) linear polarization along the axis \hat{x} , (b) for circular polarization in the $\hat{x} - \hat{y}$ plane, and (c) the same circular polarization for a somewhat larger beam waist $w = 2.22\lambda$. On the two-dimensional plot for the scaled atom number and scaled intensity variables (“phase diagram”), border points of the stability region are shown for three different cutoff parameters ($r_0/\lambda = 0.02, 0.04$ and 0.08). Convergent iterative solution of Eq. (16), i.e., stable cloud, exist in the region *below* the points. In all three phase diagrams of Fig. 1, the border points can be well fitted by a power law dependence of the critical scaled intensity on the scaled atom number, $\mathcal{I} \propto \mathcal{N}^{-c}$. The fit is represented by lines. The exponent depends on the configuration: it is $c = 0.30$ for linear and $c = 0.43$ for the circular polarization in a $w/\lambda = 1.33$ trap, and $c = 0.38$ for somewhat larger beam

waist $w/\lambda = 2.22$. We note that a Gaussian ansatz for the distribution $p(x)$ in Eq. (16) would result in an exponent $c = 0.5$ which is a quite poor approximation. That is, even if the cloud is confined in the harmonic regime of the trap, the dipole-dipole interaction creates a MF potential significantly different from a harmonic one.

Note that the exponent is essentially independent of the specific choice of the cutoff parameter r_0 in the lower bound of the integral in Eq. (15). This is a very important feature demonstrating the consistency of our model. The excluded sphere with radius r_0 obviously has an effect on the depth of the MF dipole-dipole potential. The larger the cutoff parameter r_0 , the weaker the dipole-dipole attraction in the center, thus the stability limit shifts to higher \mathcal{I} and \mathcal{N} for increasing r_0 .

There are two types of deviation from the simple power law dependence (straight line in the log-log plot). First, the boundary lines bend below the straight line at the right-most end ($\mathcal{I} \sim 1$). This happens below a certain intensity, when the trap is not deep enough to collect most of the atoms. The tail of the distribution due to untrapped and escaping atoms is folded back on the calculated area, and artificially increases the density in the center. This indicates the limits of the simulation method (need for monitoring larger spatial area). Second, for very large scaled intensity, the atoms are so strongly localized along the axis z that the hard sphere radius r_0 becomes comparable with the cloud size. This can be best seen in Fig. 1b, where the curve corresponding to the largest cutoff parameter $r_0/\lambda = 0.08$ deviates significantly from the straight line in the upper-left corner of the plot. The discussion of this extreme regime is beyond the scope of this paper.

The choice of the cutoff parameter limits the maximum localization, i. e., the maximum intensity \mathcal{I} , our approach is suitable for. Within the validity of the model the stability boundary on the $\mathcal{I} - \mathcal{N}$ phase diagram follows a power law dependence. This is also valid for strong localization where the cloud is entirely confined in the harmonic regime of the mode function. Hence we expect that the power law dependence could be extrapolated for larger scaled intensities which are allowed for atoms with smaller cutoff radius r_0 .

The dipole-dipole coupling enhances the trap depth in the center and increases the atom density there. The resulting self-contraction of the cloud is counteracted by the random motion of the atoms. We expect that instability occurs when the energy shift due to the dipole-dipole coupling exceeds the thermal energy of the atoms ($k_B T/2$ in every direction). The numerical approach has allowed us to confirm this expectation: we found that the necessary condition of the instability is $V_{dd} = k_B T/2$. In Fig. 2 the ratio of the dipole-dipole interaction potential and the thermal energy is plotted on a semi-logarithmic scale at the edge of the stable region (where still stable solution exists), and this quantity is constant close to 0.5.

Due to the integral form of the dipole-dipole potential,

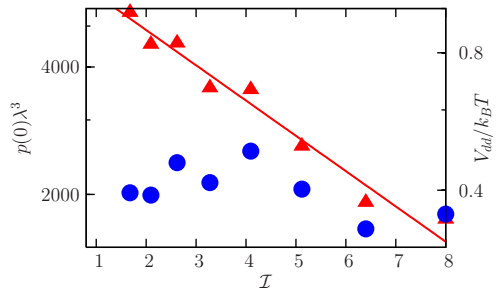


FIG. 2: Triangles with a fitted straight line are the maximum density of the cloud, $p(0)$ in units of $1/\lambda^3$, plotted against the scaled intensity \mathcal{I} at a scaled atom number \mathcal{N} slightly below the critical one. Scattered points are the minimum of the induced MF dipole-dipole potential $V_{dd}/k_B T$ calculated again at the boundary of the range of stability. The beam waist is $w/\lambda = 1.33$ and the radius of the hard sphere potential is $r_0/\lambda = 0.02$.

it seems very difficult to express the instability condition $V_{dd} = k_B T/2$ in terms of \mathcal{I} and \mathcal{N} analytically. As was mentioned previously, the distribution is not Gaussian but a rather non-trivial function of the two dimensionless parameters. Therefore the peak spatial density at the trap center, and its scaling with \mathcal{I} and \mathcal{N} , can be found only numerically. The result is shown in Fig. 2, where the peak density along the critical line of Fig. 1b is plotted together with a fixed exponential function. Obviously, both increasing the trap depth (at fixed temperature) and increasing the absolute atom number (at fixed detuning) lead to an increase of the density. However, as shown in the figure, the critical behavior can be induced at different peak densities depending on how it is obtained: whether by increasing \mathcal{I} or \mathcal{N} . At large \mathcal{I} , the instability is reached at lower atom densities in the center.

The peak density is a key parameter with respect to reaching quantum degeneracy, which is roughly at $p(0)\lambda_{\text{deBroglie}}^3 \approx \zeta(3/2) = 2.612$ [31]. Considering the numerical values of the peak density at the limit of the dipole-dipole instability in Fig. 2, one can conclude that Bose-Einstein condensation could be reached if the absolute temperature is below $100 \mu\text{K}$. In this case the assumption of a Boltzmann distribution in Eq. (16) is obviously wrong. The order of the limit of reaching quantum degeneracy and that of the dipole-dipole instability depends on the working point, the absolute value of the temperature and the dipole trap depth. For a deep enough trap potential, e.g., in the range of mK, the full range of the scaled intensity \mathcal{I} shown in the plots corresponds to much higher temperatures than $100 \mu\text{K}$. The classical gas assumption is consistent and the dipole-dipole instability should occur in this case.

Finally, we discuss the validity of the effective Hamiltonian given in Eq. (13) which keeps only the leading order term of the dipole-dipole interaction. The phase diagram

of Fig. 3, similar to those in Fig. 1, shows that the boundary calculated from the approximative Hamiltonian (13) can be significantly shifted from the one derived from the full two-body Hamiltonian (19) (this latter is represented by lines connecting the data points of Fig. 1b, the points are removed). The difference occurs for the small-

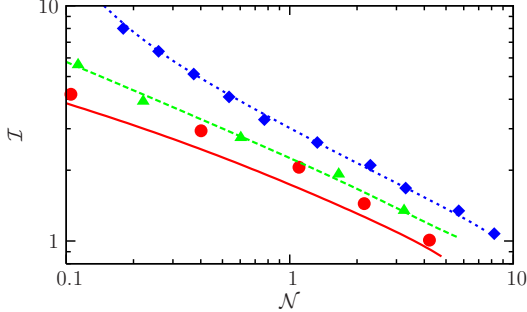


FIG. 3: The stability limits of the atomic cloud (lines) are compared to the ones gained from the approximate first order interaction described by Eq. (15), (circles for $r_0/\lambda = 0.02$, triangles for $r_0/\lambda = 0.04$ and diamonds for $r_0/\lambda = 0.08$). The beam waist is $w/\lambda = 1.33$.

est value of the cutoff parameter, $r_0/\lambda = 0.02$, when the small hard sphere radius allows for large β values in the power series of Eq. (12). For the other two parameters, $r_0/\lambda = 0.04$ and $r_0/\lambda = 0.08$, the zeroth-order Hamiltonian produces perfectly acceptable results.

Although the effective Hamiltonian given in Eq. (13) may fail to predict the position of the boundary in the phase diagram, it gives good results, e.g., for the cloud shape, inside the stability region. This can be understood from Fig. 4 which depicts the ratio of the MF dipole-dipole potential to the total potential at the center of the cloud. This is the same ratio as that of the higher order terms of (19) to the first order one in (13). The

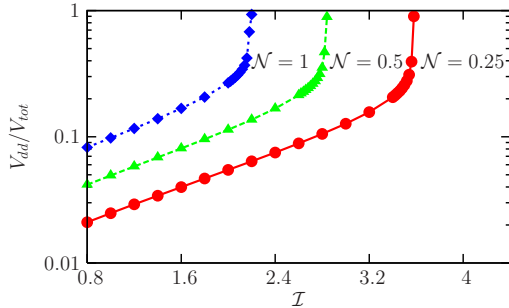


FIG. 4: The ratio of the MF dipole potential and the total potential (compared at their minimum) as a function of the scaled intensity I for $w/\lambda = 1.33$ at fixed values of $N = 1$, 0.5 and 0.25.

critical behavior as a function of the scaled intensity is clearly manifested in this semi-logarithmic plot: the ratio grows exponentially with the intensity and, at a critical

intensity, it jumps up to 1. The exponent of the growth increases slightly with the parameter N , it is 0.00165, 0.00170, and 0.00186 for $N = 0.25, 0.5$ and 1, respectively. The main thing to observe is that the criticality is reached at fairly low ratio of the dipole potential to the total one, at a value about 0.3. It is only in the vicinity of the critical point that the dipole-dipole term explodes and dominates the trap potential.

VII. CONCLUSION

We set up a simple but versatile model to study the stability of far-off-resonance trapping against the dipole-dipole interaction. The model can be adapted to various geometries, atomic species, polarizations, etc. We found that the radiative atom-atom interaction in the laser polarized gas can indeed produce an instability of a pancake-shaped atomic cloud. When the dipole-dipole energy shift reaches the temperature, the unbalanced attraction in the trap center yields a collapse of the cloud. The condition for the instability in terms of the atom density and the temperature is obtained numerically in the form of phase diagrams.

The density necessary for large enough dipole-dipole shift is quite large, however, the temperature is not needed to be very low so that the instability be observable. Provided the optical dipole trap is deep enough, the stability can be lost at moderate phase-space densities, well above the condensation threshold. The dipole-dipole interaction strongly dominates the influence of quantum statistics in near-resonant laser fields [32]. This is not the case for very large detunings, hence we expect that the effect of cloud instability offers parameter regimes where quantum statistical properties can be probed. This is the subject of our forthcoming research.

Acknowledgments

We thank J. Asbóth and T. Kiss for fruitful discussions and for their critical reading of the manuscript. This work was supported by the National Scientific Fund of Hungary (Contract Nos. T043079, T049234).

VIII. APPENDIX

In the Appendix we present the effective two-body Hamiltonian H_{eff} that takes into account the possibility of close pairs of atoms in a non-perturbative manner as introduced in Section III.

Inserting back the stationary adiabatic atomic polarization σ_n of Eq. (12) into the original form of the Hamiltonian of the system Eq. (3) and eliminating the appearing double sums as described in Sec. III, one can end up

with the effective two-body Hamiltonian:

$$\begin{aligned}
H_{\text{eff}} = & \sum_{n=1}^N \frac{\vec{p}_n^2}{2m} + \frac{\hbar\Omega^2}{\Delta_A} \left[\sum_n f_n^2 \right. \\
& + \sum_{\substack{n,m \\ m \neq n}} f_n^2 \left\{ (\beta'_{mn})^2 + 2\beta''_{mn} + 3(\beta''_{mn})^2 \right\} \\
& \left. - \frac{\gamma}{\Delta_A} \sum_{\substack{n,m \\ m \neq n}} f_m f_n \beta_{mn} \left\{ \left(1 + \beta''_{mn} \right)^2 + 3(\beta'_{mn})^2 \right\} \right], \tag{19}
\end{aligned}$$

where $f_n = f(\vec{r}_n)$ is the mode function of the field at the position of the n th atom, and β'_{mn} , β''_{mn} are defined as below:

$$\beta'_{mn} = \frac{\gamma}{\Delta_A} \frac{\beta_{mn}}{1 - \frac{\gamma^2}{\Delta_A^2} \beta_{mn}^2}, \tag{20}$$

$$\beta''_{mn} = \frac{\gamma^2}{\Delta_A^2} \frac{\beta_{mn}^2}{1 - \frac{\gamma^2}{\Delta_A^2} \beta_{mn}^2}. \tag{21}$$

Note that the denominator of the expressions Eq. (20) and Eq. (21) should be strictly greater than 0, due to the relation $\beta_{mn}\gamma/|\Delta_A| < 1$ that is the condition of summing up the geometric series resulting from Eq. (11).

Apart from the zeroth order effective Hamiltonian $H_{\text{eff}}^{(0)}$, Eq. (13), further terms appear in Eq. (19) in higher orders of $\beta_{mn}\gamma/\Delta_A$. The new terms have two apparent meaning: the second line of Eq. (19) renormalizes the dipole trap potential (first line), while the appearing β'_{mn} , β''_{mn} in the third line increase the strength of the dipole-dipole interaction. This increment is negligible and the zeroth order effective Hamiltonian, Eq. (13), can be used if $\beta_{mn}\gamma/\Delta_A$ is really a small parameter, however when it gets close to one, the non-perturbative form of the effective Hamiltonian, Eq. (19), should be used.

[1] R. Grimm, M. Weidemüller, and Y. Ovchinnikov, *Adv. At. Mol. Opt. Phys.* **42**, 95 (2000).

[2] D. W. Sesko, T. G. Walker, and C. E. Wieman, *J. Opt. Soc. Am. B* **8**, 946 (1991).

[3] C. G. Townsend, N. H. Edwards, C. J. Cooper, K. P. Zetie, C. J. Foot, A. M. Steane, P. Sriftgiser, H. Perrin, and J. Dalibard, *Phys. Rev. A* **52**, 1423 (1995).

[4] G. Hillenbrand, C. J. Foot, and K. Burnett, *Phys. Rev. A* **50**, 1479 (1994).

[5] D. Boiron, A. Michaud, P. Lemonde, Y. Castin, C. Salomon, S. Weyers, K. Szymaniec, L. Cognet, and A. Clairon, *Phys. Rev. A* **53**, R3734 (1996).

[6] A. M. Smith and K. Burnett, *J. Opt. Soc. Am. B* **8**, 1592 (1991).

[7] K. Ellinger, J. Cooper, and P. Zoller, *Phys. Rev. A* **49**, 3909 (1994).

[8] G. Labeyrie, F. Michaud, and R. Kaiser, *Physical Review Letters* **96**, 023003 (pages 4) (2006), URL <http://link.aps.org/abstract/PRL/v96/e023003>.

[9] T. Pohl, G. Labeyrie, and R. Kaiser, *Physical Review A (Atomic, Molecular, and Optical Physics)* **74**, 023409 (pages 4) (2006), URL <http://link.aps.org/abstract/PRA/v74/e023409>.

[10] S. J. M. Kuppens, K. L. Corwin, K. W. Miller, T. E. Chupp, and C. E. Wieman, *Phys. Rev. A* **62**, 013406 (2000).

[11] K. M. O'Hara, S. R. Granade, M. E. Gehm, and J. E. Thomas, *Phys. Rev. A* **63**, 043403 (2001).

[12] N. Schlosser, G. Reymond, and P. Grangier, *Phys. Rev. Lett.* **89**, 023005 (2002).

[13] K. A. Suominen, *J. Phys. B: At. Mol. Opt. Phys.* **29**, 5981 (1996).

[14] D. Boiron, A. Michaud, J. M. Fournier, L. Simard, M. Sprenger, G. Grynberg, and C. Salomon, *Phys. Rev. A* **57**, R4106 (1998).

[15] M. D. Barrett, J. A. Sauer, and M. S. Chapman, *Phys. Rev. Lett.* **87**, 010404 (2001).

[16] P. Domokos, A. Vukics, and H. Ritsch, *Phys. Rev. Lett.* **92**, 103601 (2004).

[17] A. Vukics and P. Domokos, *Phys. Rev. A* **72**, 031401(R) (2005).

[18] J. McKeever, J. R. Buck, A. D. Boozer, A. Kuzmich, H.-C. Nägerl, D. M. Stamper-Kurn, and H. J. Kimble, *Phys. Rev. Lett.* **90**, 133602 (2003).

[19] P. Maunz, T. Puppe, I. Schuster, N. Syassen, P. W. H. Pinkse, and G. Rempe, *Nature* **428**, 50 (2004).

[20] S. Nussmann, K. Murr, M. Hijkema, B. Weber, A. Kuhn, and G. Rempe, *Nature Physics* **1**, 122 (2005).

[21] S. Nussmann, M. Hijkema, B. Weber, F. Rohde, G. Rempe, and A. Kuhn, *Phys. Rev. Lett.* **95**, 173602 (2005).

[22] P. Domokos and H. Ritsch, *Phys. Rev. Lett.* **89**, 253003 (2002).

[23] A. T. Black, H. W. Chan, and V. Vuletić, *Phys. Rev. Lett.* **91**, 203001 (2003).

[24] J. K. Asbóth, P. Domokos, H. Ritsch, and A. Vukics, *Phys. Rev. A* **72**, 053417/1 (2005).

[25] J. Guo and J. Cooper, *Phys. Rev. A* **51**, 3128 (1995).

[26] R. H. Lehmberg, *Phys. Rev. A* **2**, 883 (1970).

[27] S. Giovanazzi, A. Gorlitz, and T. Pfau, *Physical Review Letters* **89**, 130401 (pages 4) (2002), URL <http://link.aps.org/abstract/PRL/v89/e130401>.

[28] J. Stuhler, A. Griesmaier, T. Koch, M. Fattori, T. Pfau, S. Giovanazzi, P. Pedri, and L. Santos, *Physical Review Letters* **95**, 150406 (pages 4) (2005), URL <http://link.aps.org/abstract/PRL/v95/e150406>.

[29] D. Nagy, J. K. Asbóth, P. Domokos, and H. Ritsch, *Eur. Phys. Lett.* **74**, 254 (2006).

[30] J. H. Wesenberg and K. Molmer, *Physical Review Letters* **93**, 143903 (pages 4) (2004), URL <http://link.aps.org/abstract/PRL/v93/e143903>.

[31] Y. Castin, in *Coherent atomic matter waves*, edited by R. Kaiser, C. Westbrook, and F. David (EDP Sciences and Springer Verlag, 2001), pp. 1–136.

[32] C. Menotti and H. Ritsch, *Physical Review A (Atomic, Molecular, and Optical Physics)* **60**, R2653 (1999), URL <http://link.aps.org/abstract/PRA/v60/pR2653>.